ELSEVIER

Applied Surface Science 86 (1995) 303–309

applied surface science

Influence of temperature gradient to solidification velocity ratio on the structure transformation in pulsed- and CW-laser surface treatment

N.A. Berjeza [a], S.P. Velikevitch [a], V.I. Mazhukin [b], I. Smurov [c], G. Flamant [d,*]

[a] *Physical Technical Institute, Byelorussian Academy of Science, Zhodinskaya St. 4, 220730 Minsk, Belarus*
[b] *Institute of Mathematical Modeling, Russian Academy of Science, Miusskaya square, 4, 125047 Moscow, Russian Federation*
[c] *Ecole Nationale d'Ingénieurs de Saint-Etienne, 58, rue Jean Parot, 42023 Saint-Etienne Cedex, France*
[d] *Institute de Science et de Génie des Matériaux et Procédés, CNRS, B.P. 5, 66125 Font-Romeu Cedex, France*

Received 27 May 1994; accepted for publication 20 September 1994

Abstract

The temperature gradient G, the solidification velocity R, and the G/R ratio are used in solid–liquid interface analysis. The critical G/R values characterizing the transitions from a planar front to a cellular structure, and from a cellular to cellular-dendritic structure during solidification are determined. The regularities of the rapid solidification process are shown on the example of the titanium alloy subjected to boriding with a CW-laser. The G/R ratio and cooling rate values versus molted zone depth are analyzed. The dependence of the relative transition depth from cellular to cellular-dendritic structure on laser beam velocity is determined.

1. Introduction

The liquid–solid interface morphology determines the microstructure of the remelted zone, governing the material properties. It is presently the subject of investigation for high cooling rates and large temperature gradients typical for laser treatment [1–4].

For low rate (10^{-4}–10^{-2} cm/s) solidification processes in binary alloys, the G/R value (the ratio of the temperature gradient to solidification front velocity) was found to be a governing parameter when turning from a planar front into a cellular structure [5]. As for transition from a cellular to dendritic structure, the $(G/R)^{1/2}$ value was found to be the governing parameter for directional solidification in dilute alloys [6].

In Ref. [1] it was shown that at high solidification rate (1–10^2 cm/s), typical of laser-irradiated Ni alloys, the decrease in G/R may lead to the following changes in the morphological structure of the solid–liquid interface: a planar front → cellular → cellular dendrites → dendrites.

2. Simplified models for G/R calculation

To determine the G/R value in a general case of laser alloying (remelting), one needs to solve a rather complicated problem taking into account the following physical phenomena: heating, melting, convective heat and mass transfer, solidification. At present

* Corresponding author. Fax: +33 68 302940.

SSDI 0169-4332(94)00446-3

only several particular cases are analyzed [7–9] and the utilized mathematical methods are rather complicated.

In this paper the simplest approach, the simplest mathematical models to calculate the G/R values are proposed. Only two phenomena are taken into account: (a) surface heating; (b) heat transfer into the bulk of metal. As a result simple analytical solutions are obtained, that link the treatment parameters, material properties and G/R value.

2.1. Pulsed-laser treatment

The key assumption, made to justify the approximated calculation procedure, is to neglect the latent melting heat. This assumption considerably simplified the problem – by 'withdrawing' it from the Stefan-type problems and relating it to the problems of surface heating without phase transition.

The thermophysical properties of the material are assumed to be approximately the same in solid and liquid states. The material is considered to be a homogeneous semi-infinite solid. The density of energy distribution over the spot and during the pulse duration was assumed constant. Cooling of the melted metal is realized only due to thermal conduction. One-dimensional approximation is considered, i.e. the laser beam diameter is larger than the heat effected zone.

The solution of this problem for heating ($t \leqslant \tau$) and cooling ($t > \tau$, $\gamma = t - \tau$) has the form [1,10]:

for $t \leqslant \tau$:

$$T(z,t) = \frac{q_0}{\lambda}\left\{\left(\frac{4at}{\pi}\right)^{1/2}\exp\left[-\left(\frac{z}{(4at)^{1/2}}\right)^2\right] - z\,\mathrm{erfc}\left(\frac{z}{(4at)^{1/2}}\right)\right\} + T_0, \tag{1}$$

for $t > \tau$, $\gamma = t - \tau$:

$$T(z,t) = \frac{q_0}{\lambda}\left\{\left(\frac{4at}{\pi}\right)^{1/2}\exp\left[-\left(\frac{z}{(4at)^{1/2}}\right)^2\right] - \left(\frac{4a\gamma}{\pi}\right)^{1/2}\exp\left[-\left(\frac{z}{(4a\gamma)^{1/2}}\right)^2\right] - z\left[\mathrm{erfc}\left(\frac{z}{(4at)^{1/2}}\right) - \mathrm{erfc}\left(\frac{z}{(4a\gamma)^{1/2}}\right)\right]\right\} + T_0. \tag{2}$$

The values for the temperature gradient $G(z, t)$ and cooling rate $\dot{T}(z, t)$ for the cooling period $t > \tau$ are derived from (4):

$$G(z,t) = \frac{\partial T}{\partial z} = -\frac{q_0}{\lambda}\left[\mathrm{erfc}\left(\frac{z}{(4at)^{1/2}}\right) - \mathrm{erfc}\left(\frac{z}{(4a\gamma)^{1/2}}\right)\right], \tag{3}$$

$$\dot{T}(z,t) = \frac{\partial T}{\partial t} = \frac{q_0}{\lambda}\left\{\left(\frac{a}{\pi t}\right)^{1/2}\exp\left[-\left(\frac{z}{(4at)^{1/2}}\right)^2\right] - \left(\frac{a}{\pi\gamma}\right)^{1/2}\exp\left[-\left(\frac{z}{(4a\gamma)^{1/2}}\right)^2\right]\right\}, \tag{4}$$

$$\dot{T} = G \cdot R. \tag{5}$$

2.2. CW-laser treatment

In case of continuous laser treatment thermal processes can be described by means of the model [11,12], where temperature fields generated in the semi-infinite domain by the Gaussian surface heat source $q = q_{ef}\exp[-(x^2+y^2)/R_{ef}]$ moving along the x-axis with velocity V can be determined from the steady-state heat transfer equation. In the coordinate system associated with the moving beam the problem is formulated as follows:

$$a\Delta T + V\nabla_x T = 0, \quad x, y \in (-\infty, \infty), \quad z \in (0, \infty),$$

$$\lambda\nabla_z T\,|_{z=0} = -q_{ef}\exp\left[-\left(\frac{x^2+y^2}{R_{ef}^2}\right)\right],$$

$$q_{ef} = \frac{P_{ef}}{\pi R_{ef}^2},$$

$$T\,|_{x=\pm\infty} = T\,|_{y=\pm\infty} = T\,|_{z=\infty} = T_0. \tag{6}$$

In dimensionless coordinates and functions

$$f=(T-T_0)\frac{\lambda\pi R_{ef}}{P_{ef}},\qquad \rho=\frac{R_{ef}V}{4a},$$

$$x'=x/R_{ef},\qquad y'=y/R_{ef},\qquad z'=z/R_{ef}$$

the solution of the problem (6) can be presented in the form of the well known integral [11,12]:

$$f(x',\,y',\,z',\,\rho)=\frac{1}{\pi}\int_0^\infty \exp\left(-\frac{(x'+\rho\mu^2)^2+y'^2}{1+\mu^2}-\frac{z'^2}{\mu^2}\right)\times\frac{d\mu}{1+\mu^2}. \tag{7}$$

However direct application of the formula (7) for computations is not convenient because of a number of reasons. The main of them are pointed out below.

(1) In the case $\mu\to 0$ the rapidly decreasing function $e^{-z'^2/\mu^2}$ is dominant, that places stiff limitations on the integration step. When $\mu\to\infty$ the computation process must be restricted by some large value of μ, but error estimation for this operation is complicated because of a large number of parameters $(x',\,y',\,z',\,\rho)$.

(2) Procedure of determining of isotherm, temperature maximum and x'-coordinate of the maximum depending on the velocity ρ is cumbersome.

(3) There are some computational difficulties in determining the temperature fields for planes $y'=\text{const}\neq 0$ and for small values of ρ.

To eliminate the above mentioned problems it is more convenient to express the solution of the problem (6) as a product of two functions:

$$f(x',\,y',\,z',\,\rho)=g(r,\,z',\,\rho)\,\exp(\rho^2-2\rho x'). \tag{8}$$

Here $g(r,\,z',\,\rho)$ describes the axi-symmetric component of the temperature field and the second term $\exp(\rho^2-2\rho x')$ describes additional asymmetric perturbation, which is proportional to the asymmetric term $\exp(-2\rho x')$. The $g(r,\,z',\,\rho)$ function can be written in the form of an integral

$$g(r,\,z',\,\rho)=\int_0^\infty f_1(r,\,u)f_2(z',\,\rho,\,u)\,du, \tag{9}$$

where the $f_1(r,\,u)=J_0(2ru)$ is the well-known Bessel function, and

$$f_2(z',\,\rho,\,u)=\frac{u}{(\rho^2+u^2)^{1/2}}\exp\left[-u^2-2z'(\rho^2+u^2)^{1/2}\right].$$

The solution in the new form is written as follows:

$$f(x',\,y',\,z',\,\rho)=\exp(\rho^2-2\rho x')\int_0^\infty\frac{u}{(\rho^2+u^2)^{1/2}}\times\exp\left[-u^2-2z'(\rho^2+u^2)^{1/2}\right]J_0(2ru)\,du. \tag{10}$$

The proposed form of the solution is convenient for numerical computations and eliminate the above mentioned problems.

The absolute value of the interface velocity in the fixed (laboratory) coordinate system $(x,\,y,\,z)$ is equal to the normal velocity of the substance 'flowing' through the interface in the $(x',\,y',\,z')$ coordinate system associated with the moving beam:

$$R=V\cos\,\alpha=V\frac{|\nabla_x T|}{|\nabla T|}\bigg|_{T=T_s}=V\frac{|\partial T/\partial x|}{|\nabla T|}\bigg|_{T=T_s}. \tag{11}$$

The G/R value at the solidification interface has the form:

$$\frac{G}{R}\bigg|_{T=T_s}=\frac{|\nabla T|^2}{V|\nabla_x T|}\bigg|_{T=T_s}=\frac{(\partial T/\partial x)^2+(\partial T/\partial y)^2+(\partial T/\partial z)^2}{V|\partial T/\partial x|}\bigg|_{T=T_s}=\frac{T_s-T_0}{R_{ef}V}\times\left(\frac{1}{f}\frac{(\partial f/\partial x')^2+(\partial f/\partial y')^2+(\partial f/\partial z')^2}{|\partial f/\partial x'|}\right)\bigg|_{f=f_s}. \tag{12}$$

The model assumes the overcooling value at the liquid–solid interface to be low. The cooling rate at the solidification front is expressed by

$$\dot{T}\,|_{T=T_s} = \frac{\partial T}{\partial t}\Big|_{T=T_s} = -G\cdot R\Big|_{T=T_s} = \frac{(T_s - T_0)V}{R_{ef}}\left(\frac{1}{f}\frac{\partial f}{\partial x'}\right)_{f=f_s}. \quad (13)$$

For the $y' = 0$ plane the G/R expression simplifies and in the coordinate system $(r = x' - \rho,\ z')$ has the form:

$$\left.\frac{G}{R}\right|_{y'=0,f=f_s} = \frac{T_s - T_0}{R_{ef}V}\left(\frac{1}{f_0}\frac{(\partial f_0/\partial r)^2 + (\partial f_0/\partial z')^2}{|\partial f_0/\partial r|}\right)\Bigg|_{f_0=f_s}. \quad (14)$$

Here

$$f_0(r,\ z',\ \rho) = f(x',\ y',\ z',\ \rho)\,|_{y'=0} = \exp(-\rho^2 + 2\rho r)\int_0^\infty \frac{u}{(\rho^2+u^2)^{1/2}} \times F_{exp}J_0(2ru)\,du,$$

$$\frac{\partial f_0}{\partial z'} = -2\exp(-\rho^2+2\rho r)\int_0^\infty \frac{u}{(\rho^2+u^2)^{1/2}}F_{exp} \times J_0(2ru)(\rho^2+u^2)^{1/2}\,du,$$

$$\frac{\partial f_0}{\partial r} = \frac{2}{r}\exp(-\rho^2+2\rho r)\int_0^\infty \frac{u}{(\rho^2+u^2)^{1/2}}F_{exp} \times J_0(2ru)\left(\rho r - 1 + u^2 + z'\frac{u^2}{(\rho^2+u^2)^{1/2}} + \frac{u^2}{(\rho^2+u^2)^{1/2}}\right)du,$$

$$F_{exp} = \exp\left[-u^2 - 2z'(\rho^2+u^2)^{1/2}\right]. \quad (15)$$

3. Results and discussion

3.1. Pulsed-laser treatment

Consider pulsed-laser irradiation of Armco-iron ($\lambda = 0.46$ W/cm · K, $a = 0.092$ cm^2/s). Three pairs of values for q_{abs} and τ where chosen in such a way that the initial melt depth H ($H = 24$ μm) is the same:

(1) $q_{abs} = 5\times10^5$ W/cm^2, $\tau = 8.9\times10^{-5}$ s;

(2) $q_{abs} = 5\times10^4$ W/cm^2, $\tau = 2.5\times10^{-3}$ s;

(3) $q_{abs} = 5\times10^3$ W/cm^2, $\tau = 1.2\times10^{1}$ s.

For all cases the values of temperature gradient G, cooling rate $\dot{T}$, solidification velocity R and ratio G/R on the interface were calculated from (3)–(5), Fig. 1.

The plots should be read from the right to the left since $z/H = 1$ corresponds to the start of solidification while $z/H = 0$ corresponds to its end. The G, $\dot{T}$, G/R values are, in fact, negative for the solidification process but for the convenience are shown as

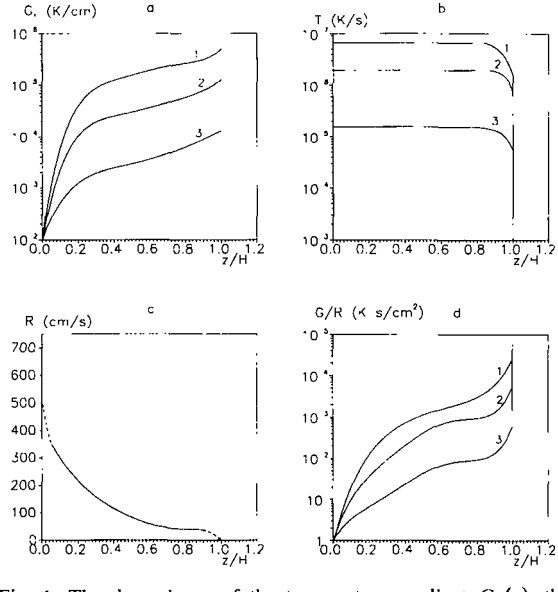

Fig. 1. The dependence of the temperature gradient G (a), the cooling rate $\dot{T}$ (b), the solidification interface velocity R (c) and the ratio G/R (d) at the solidification interface in Armco-iron versus dimensionless melt depth z/H for the following values of absorbed power density: (1) $q_{abs} = 5\times10^5$ W/cm^2; (2) $q_{abs} = 5\times10^4$ W/cm^2; (3) $q_{abs} = 5\times10^3$ W/cm^2 ($H = 24$ μm).

positive. Fig. 1a shows the temperature gradient at the solidification interface to be maximum at the initial moment of solidification and to approach zero at the end. As indicated by Figs. 1a, 1b, 1d for the fixed initial depth of the melted layer H, the temperature gradient G, cooling rate $\dot{T}$ and G/R values are directly proportional to the absorbed power density q_{abs}. At the onset of solidification the cooling rate $\dot{T}$ 'starts' from zero, then increases abruptly, and finally at $z/H = 0.8$ achieves a constant value, Fig. 1b. The solidification velocity R is practically independent of q_{abs}, Fig. 1c. In Armco-iron, with the solidification interface moving towards the surface, R increases from 0 (at $z/H = 1$) to 40 cm/s ($z/H = 0.9$) achieving hundreds of centimeters per second at $z/H \to 0$. The heat transfer model used is rather rough and, as shown in Ref. [4], with the latent heat of solidification taken into account, the R value by reaching the 'plateau' (40 cm/s for Armco-iron) remains constant up to the end of the solidification process. Fig. 1d shows that the G/R value starts to change from ∞ at the onset of solidification ($R = 0$, G is at maximum) approaches 0 (since $G \to 0$ and R is at maximum) at the end of solidification.

3.2. CW-laser treatment

Calculations for the Ti alloy (wt%): Al 4.5, Mo 2.0, V 4.5, Cr 1.0, Fe 0.6 ($\lambda = 0.21$ W/cm · K, $a = 0.07$ cm^2/s, $T_{melt} = 1933$ K) were performed for the three groups of laser beam parameters (Table 1). Numerical results were obtained from (11)–(14).

Common behavior of the G/R value at the solidification interface appears to be approximately the same for continuous (Fig. 2a) and pulsed (Fig. 1d) laser treatment. At the onset of solidification the G/R value is maximum. At z/H reducing from 1.0 to 0.9, G/R decreases first abruptly and later smoothly up to a certain finite V-dependent value. As evident from Fig. 2a, G/R is dependent on the laser beam velocity V: the values of G/R are smaller for the larger values of V.

The dependence of the cooling rate $\dot{T}$ on z/H at the solidification interface for continuous laser treatment (Fig. 2b) coincides with that for pulsed-laser treatment (Fig. 1b).

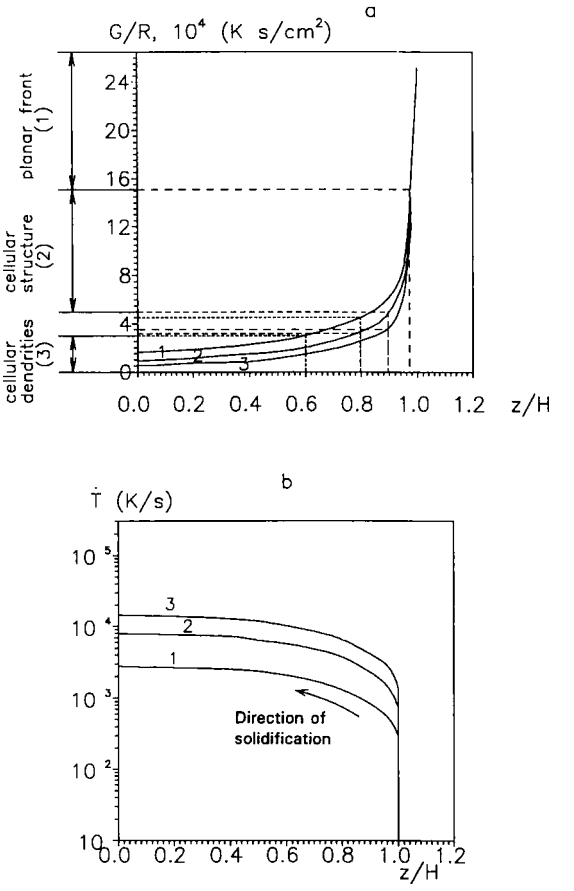

Fig. 2. The dependence of G/R (a) and $\dot{T}$ (b) versus dimensionless melt depth z/H at the interface in the plane $y = 0$: (1) $V = 0.5$ m/min, (2) $V = 1.0$ m/min, (3) $V = 2.0$ m/min.

Table 1
The values of the P_{ef} and R_{ef} parameters for Gaussian surface heat source for different velocities of laser beam

Experimental				Calculated	
Laser beam velocity V (m/min)	Laser beam power P (kW)	Depth of melted zone H (mm)	Width of melted zone D (mm)	Effective power of source P_{ef} (kW)	Effective radius of source R_{ef} (mm)
0.5	1	0.550	1.950	0.264	0.767
1.0	1	0.375	1.500	0.235	0.668
2.0	1	0.280	1.400	0.292	0.755

4. G/R critical values

In the experiment, the specimens of the annealed titanium alloy (wt%) Al 4.5, Mo 2.0, V 4.5, Cr 1.0, Fe 0.6, previously coated with amorphous boron powder, were irradiated with a continuous CO_2-laser in argon environment. The parameters are reported in Table 1. Each laser-affected specimen was cut normal to the direction of the laser beam motion. Then the depths of the transitions from one type of structure to another were measured.

The transition from a planar front to a cellular structure was distinctly observed for the laser beam velocity $V = 0.5$ m/min. The structure with the planar front is 17 μm thick. The transition from this type of structure to a cellular one was observed at a dimensionless depth of 0.97.

For $V = 1.0$ m/min, the morphological instability of the solidification interface is highly pronounced. Transitions depths are shown in Fig. 3 (transition from a planar interface to a cellular structure and from a cellular to cellular-dendritic structure). The relative depths of transition are as follows: 0.6–0.8 ($V = 0.5$ m/min), 0.8–0.9 ($V = 1$ m/min), 0.9 ($V = 2$ m/min).

The depth of the transition from cellular to cellular-dendritic structure depends on the laser beam velocity, so the transition depth is decreasing with the beam velocity.

Using the measured values of transition depth, we plot the corresponding dimensionless depths values on the z/H axis of the G/R versus z/H plot (Fig. 2a). The $(G/R)_{cr}$ value is further determined from the plot.

Thus, for the considered titanium alloy the region of the solidification planar front lies above $(G/R)_{cr1} = 1.5 \times 10^5$ K s/cm^2; the 5.3×10^4–1.5×10^5 K s/cm^2 range corresponds to the zone of cellular structures and the range $(G/R)_{cr2} = 3.0 \times 10^4$–$5.3 \times 10^4$ K s/cm^2 is related to the transition from a cellular to cellular-dendritic structure.

5. Nomenclature

T, T_s, T_0 – temperature, temperature of solidification, initial temperature

λ, a – thermal conductivity and thermal diffusivity

τ – laser pulse duration, $q(z, t)$ – internal heat source

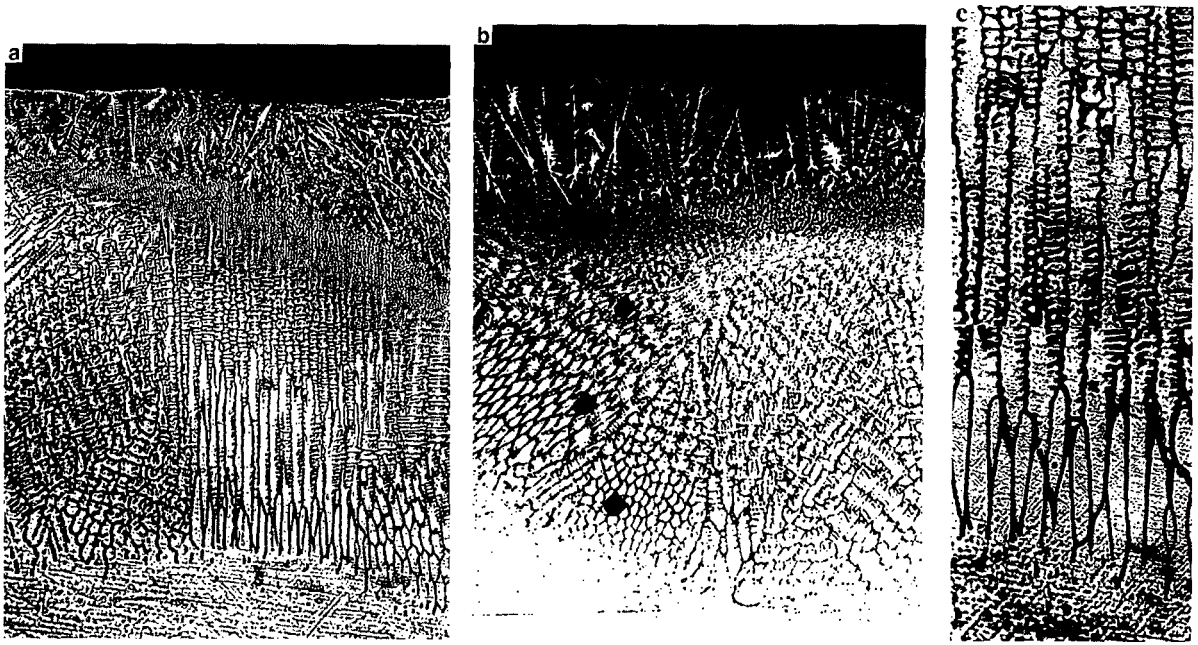

Fig. 3. Microstructure of titanium alloy after laser boriding with 1 kW power; (a) $V = 1.0$ m/min (×200), (b) $V = 0.5$ m/min (×150), (c) $V = 1.0$ m/min (×1000).

q_{abs} – density of absorbed power
H, D – initial depth and width of melt
f, f_s – dimensionless temperature and temperature of solidification
f_0 – dimensionless temperature on the $y = 0$ plane
R_{ef}, P_{ef} – efficient radius and absorbed power of Gaussian source
q_{ef} – density of efficient absorbed power
$\boldsymbol{V}$ – velocity of laser beam, $V = |\boldsymbol{V}|$, ρ – dimensionless velocity
$\boldsymbol{G} = \nabla T$ – temperature gradient, $G = |\boldsymbol{G}|$
$\boldsymbol{R}$ – normal velocity of the interface, $R = |\boldsymbol{R}|$
α – angle between $\boldsymbol{V}$ and $\boldsymbol{R}$
$\mathrm{erf}(x) = 1 - \mathrm{erfc}(x) = 2/\pi^{1/2}\int_0^x \exp(-t^2)\,\mathrm{d}t$ – error function
For any Cartesian coordinate system (x_1, x_2, x_3) and ist orthonormal unit vector system $(\boldsymbol{e}_1, \boldsymbol{e}_2, \boldsymbol{e}_3)$
$\Delta = \sum_{i=1}^{3} \partial^2/\partial x_i^2$ – Laplace operator
$\nabla = \sum_{i=1}^{3} \nabla_{x_i} \cdot \boldsymbol{e}_i = \sum_{i=1}^{3} \partial/\partial x_i \cdot \boldsymbol{e}_i$ – nabla operator

References

[1] L.E. Greenwald, E.M. Breinen and B.H. Kear, in: Laser–Solid Interaction and Laser Processing (1978), Eds. S.D. Ferris, H.J. Leamy and J.M. Poate (Boston, USA, 1979) p. 189.

[2] S.A. Astapchik and N.A. Berjeza, Izv. AN BSSR, Ser. Fiz. Tech. Nauk 4 (1989) 23.

[3] R.W. Cahn and P. Haasen, Eds., Physical Metallurgy (North-Holland, Amsterdam, 1983).

[4] P.R. Strutt, B.G. Lewis and B.H. Kear, Critical Factors in Laser and Electron Beam Glazing of Materials, Eds. B.H. Kear, B.C. Giessen and M. Cohen (North-Holland, Amsterdam, 1982) p. 485.

[5] W.A.Tiller, K.A. Jackson, J.W. Rutter and B. Chalmers, Acta Metall. 1 (1953) 428.

[6] W.A. Tiller and J.W. Rutter, Can. J. Phys. 34 (1956) 96.

[7] I. Smurov and A. Lashin, in: Laser Applications in Mechanical Industry, Ed. S. Martellucci, NATO ASI Series. Ser. E 238 (1993) 231.

[8] V.R. Voller, A.D. Brent and C. Prakash, J. Heat Mass Transfer 32 (1989) 1719.

[9] V. Mazhukin, I. Smurov, G. Flamant and C. Dupuy, Thin Solid Films 241 (1994) 109.

[10] N.N. Rykalin, A.A. Uglov, I.V. Zuev and A.M. Kokora, Laser and Electron-Beam Treatment of Material (Moscow, 1985) p. 495.

[11] N.N. Rykalin, Computations of Thermal Processes in Welding (Moscow, 1951).

[12] H.E. Cline and T.R. Anthony, J. Appl. Phys. 48 (1977) 3895.